Journal of Materials Chemistry A

Accepted Manuscript

ROYAL SOCIETY OF CHEMISTRY

www.rsc.org/materialsA

Journal of Material Chemistry A

Paper

Ultrathin Au nanowires supported on rGO/TiO_2 as an efficient photoelectrocatalyst

Received 00th January 20xx,
Accepted 00th January 20xx

DOI: 10.1039/x0xx00000x

www.rsc.org/

A Leelavathi,[a] Giridhar Madras[b] and N Ravishankar*[c]

We report the synthesis of stable graphene oxide rGO/TiO_2/Au nanowire hybrids showing excellent electrocatalytic activity for ethanol oxidation. Phase-pure anatase TiO_2 nanoparticles (~ 3 nm) were grown on GO sheets followed by the growth of ultrathin Au nanowires leading to the formation of a multidimensional ternary structure (0-D TiO_2 and 1-D Au on 2-D graphene oxide). The oleylamine used for the synthesis of the Au nanowires not only leads to stable Au nanowires anchored on the GO sheets but also leads to the functionalization and room temperature reduction of GO. Using control experiments, we delineate the role of the three components in the hybrid and show that there is a significant synergy. We show that the catalytic activity for ethanol oxidation primarily stems from the Au nanowires. While TiO_2 triggers the formation of oxygenated species on the Au nanowire surface at a lower potential and also imparts photoactivity, rGO provides a conducting support to minimize the charge transfer resistance in addition to stabilizing the Au nanowires. Compared with nanoparticle hybrids, the nanowire hybrids display a much better electrocatalytic performance. In addition to high efficiency, the nanowire hybrids also show a remarkable tolerance towards H_2O_2. While our study has a direct bearing on fuel cell technology, the insights gained are sufficiently general such that they provide guiding principles for the development of multifunctional ternary hybrids.

Introduction

Gold and its alloys have been extensively used as catalysts for a wide range of reactions for energy generation and environmental protection.[1] For these applications, controlling the size,[2] shape[3] and composition of the catalyst[4] is critical for enhancing the catalytic performance. The activity of Au catalysts is usually explained in terms of an electronic effect (d-band position), that directly influences the interaction of the reactant molecules with the catalyst surface.[5] However, an inherently low binding energy of oxygen species on Au surface is a major limiting factor for various oxidation reactions.[6] The electrocatalytic oxidation of alcohols is regarded to be ideal for portable power applications owing to the high energy conversion efficiency; however, this reaction requires an optimum adsorption of oxygenated species on Au catalyst.[7] To achieve this, the most widely used strategy is to design a bimetallic catalyst of Au alloyed with oxophilic metals that may significantly enhance the reaction kinetics.[8, 9] The key problem involved in these bimetallic catalysts is the dissolution of the lesser noble metal in the electrolyte during operation that leads to compositional changes and is detrimental for the long-term stability of the catalyst.[4] To solve the aforementioned issues, oxide-supported monometal nanostructures are ideal, based on both electronic and bifunctional effects of support.[10, 11] Furthermore, the strong metal-support interaction promotes the oxidation reaction, due to the modified electronic structure of Au.[12] Recently, it has been proposed that the metal oxide support could enhance the performance of ethanol fuel cell by weakening the C-C bond.[7, 13] It is generally accepted that the oxide-gold interface plays a significant role in the catalytic performance.[12, 14] TiO_2 has emerged as a promising substrate because of inherent optoelectronic properties that is expected to further stimulate the performance of the catalyst via photoexcitation.[15] However, the low conductivity of TiO_2 and high rates of charge recombination is a disadvantage for practical applications and thus the design of a different type of support is needed.[16, 17]

The toolbox to tackle the above-mentioned problems is rich and includes the modification of the metal oxide with carbon supports[18,19] that are capable of providing high conductivity and good dispersion of the oxide. Over the past few years, reduced graphene oxide (rGO) has emerged as a potential support because of its anchoring ability towards catalyst particles arising from the functional groups on its surface.[20, 21, 22] A judicious combination of TiO_2 and rGO is attractive,[23, 24] as it could potentially suppress the recombination of photogenerated charge carriers and can serve as a highly conducting support material for fuel cell.[25]

[a] Centre for Nanoscience and Engineering, Indian Institute of Science, Bangalore-560012, India.
[b] Department of Chemical Engineering, Indian Institute of Science, Bangalore-560012, India.
[c] Materials Research Centre, Indian Institute of Science, Bangalore-560012, India. Email: nravi@mrc.iisc.ernet.in

†Electronic Supplementary Information (ESI) available. See DOI: 10.1039/x0xx00000x

The electrocatalytic alcohol oxidation using Au as the catalyst is sensitive to the structure of the gold surface.[3] In case of ultrathin nanowires, a significant fraction of the atoms reside on the surface and contribute to subtle changes in the electronic structure due to relaxation.[26] Thus, it would be interesting to investigate the use of Au nanowire as a potential candidate for electrocatalytic reactions.[27, 28] Indeed, recent work using Au nanowires (AuNW) has demonstrated a negative shift in the redox potential of ferri/ferro-cyto-c as well as exceptional performance for electrocatalysis.[29, 30] In this study, we use ultrathin Au nanowires synthesized using wet chemical means[31, 32, 33] as a catalyst for alcohol oxidation reactions. We use TiO_2 nanoparticles supported on reduced graphene oxide as the support to grow the ultrathin AuNW and demonstrate a synergistic coupling effect in the multidimensional ternary catalyst involving 0-D TiO_2, 1-D AuNW and 2-D rGO. We also synthesize the binary counterparts to delineate the contribution of each of the components to the overall performance of the hybrid. The ternary hybrid architecture exhibited promising electrochemical activity due to the synergy by utilizing incipient oxide formation on Au nanowires coupled with the higher electrical conductivity from rGO. The supported AuNW exhibited higher electrocatalytic activity than nanoparticle hybrids and also better tolerance against H_2O_2 crossover effects. To further improve the performance, we have coupled the optoelectronic properties of TiO_2 with electrocatalytic properties of AuNW and demonstrate an improvement in the photo-assisted electrocatalytic activity in the ternary hybrid. Considering its superior performance, particularly photo-assisted electrocatalytic activity, tolerance and stability, rGO/TiO_2/AuNW appears to be a promising candidate for photofuel cells.

Results and discussion

Growth of ultrathin Au nanowires on supports

The preparation of ternary rGO/TiO_2/AuNW involves two steps: deposition of TiO_2 nanoparticles on GO sheets, followed by one-pot GO reduction and growth of ultrathin high single-crystalline Au nanowires. In the first step, graphitic oxide was prepared according to modified Hummer's method,[34] and TiO_2 nanoparticles (~ 3 nm diameter) were uniformly nucleated on GO through a simple, rapid microwave technique as illustrated in Fig. 1. The XRD pattern of as-synthesized GO/TiO_2 shows peaks corresponding to pure anatase TiO_2 in addition to the intense peak of GO (Fig. S1). The morphology of the as-synthesized GO/TiO_2 was examined using electron microscopy. Fig. 2A is a representative transmission electron microscope (TEM) image that reveals a homogeneous dispersion of TiO_2 nanoparticles on the GO sheets as is also evident from the SEM image (Fig. S2). High-resolution TEM micrographs from several regions show that the titania particles are interconnected (Fig. 2B); the d-spacing of 3.5 Å matches well with the (101) spacing of the anatase phase of TiO_2 and is also consistent with XRD analysis. The formation of anatase TiO_2 was further confirmed by using Raman spectroscopy, the characteristic vibration peak for anatase was observed at 150 ($E_{g(1)}$), 396 ($B_{1g(1)}$), 513 (A_{1g}+$B_{1g(2)}$) and 639 cm^{-1} ($E_{g(2)}$) (Fig. S3),[35] along with D and G bands of GO. The average size of the TiO_2 particles is around 3 nm and is much smaller compared to the size of TiO_2 nanoparticles reported earlier.[36, 37]

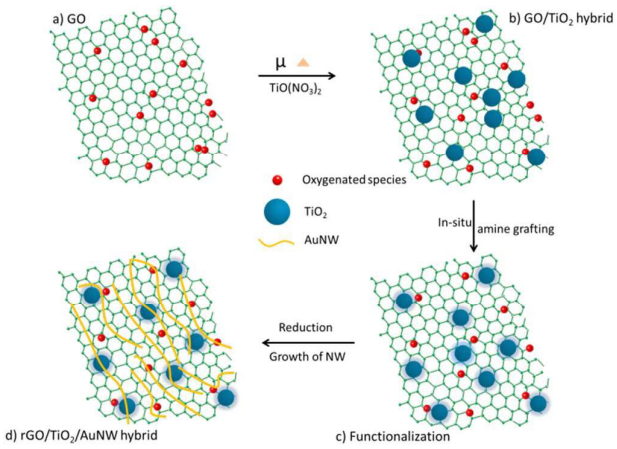

Fig. 1 Scheme for growth of ultrathin Au nanowires on rGO/TiO_2. (a) GO prepared by Hummer's method (b) nucleation of TiO_2 nanoparticles (~ 3 nm) on GO sheets via microwave synthesis (c) room temperature reduction and in-situ amine functionalization of GO, (d) functionalized substrates facilitates the growth of Au nanowires and forms multidimensional ternary hybrid rGO/TiO_2/AuNW. The hexagonal pattern in the schematic is only shown to represent rGO and is not drawn to scale.

The as-synthesized GO/TiO_2 composite was added to Au nanowire growth solution (for details, see Experimental Section). The solution mixture was sealed and undisturbed for 6 h at room temperature.[38] During this process, the presence of oleylamine (OA) leads to intercalation[39] and functionalization of GO followed by direct nucleophilic attack of the amine on epoxy group that leads to deoxygenation or reduction of GO.[40] The resulting amine-modified reduced GO (rGO) loaded with TiO_2 favors the growth of nanowires on the surface as depicted schematically in Fig. 1. TEM micrographs (Fig. 2C) of the samples display dense growth of high-aspect-ratio ultrathin Au nanowires on the rGO/TiO_2 sheets; the nanowires are well-separated and dispersed on the substrate (Fig. S4).

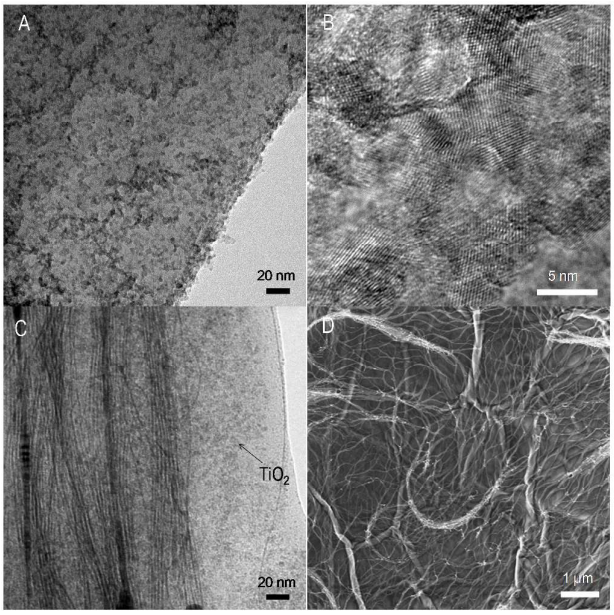

Fig. 2 (A) TEM image shows the presence of TiO_2 nanoparticles (~ 3 nm) on GO sheets synthesized using titanyl nitrate precursors. (B) HRTEM micrograph of GO/TiO_2, showing lattice spacing corresponds to the (101) anatase phase of TiO_2. (C) bright-field image showing ultrathin Au nanowires (~ 2 nm diameter) on TiO_2/rGO hybrid support (D) Low magnification SEM micrograph displays the dense and uniform growth of Au nanowires on rGO over a large area.

As control samples, binary hybrids such as rGO/AuNW and TiO_2/AuNW were also synthesized under similar conditions for a better understanding of electrochemical properties of the ternary hybrid. Incubating GO in the nanowire growth solution leads to a dense growth of ultrathin AuNW on GO sheets as seen in the SEM image (Fig. 2D). However, functionalization was required on TiO_2 for the growth of nanowires[30] (Fig. S5). TEM image (Fig. S6) illustrates the growth of nanowires on amine-modified TiO_2 nanoparticles.

X-ray photoelectron spectroscopy (XPS) analysis of rGO/TiO_2/AuNW samples was performed to confirm the oxidation states and the possible binding mechanism between the Au nanowires and the substrate. The presence of spectral peaks corresponding to N 1s (Fig. S7) confirms chemical modification of GO by nitrogen.[41] It is known that OA strongly adsorbs on the GO sheets.[39] Furthermore, C 1s spectrum of rGO/TiO_2/AuNW can be deconvoluted into several peaks at 284.5 eV (sp^2C), 285.4 eV (sp^3C or C-OH or C-N), 286.5 eV (epoxy C-O), 287.7 eV (carbonyl –C=O) and 288.8 eV (carboxylate –COO-) as shown in Fig. 3A.[42, 43, 44] Compared with the C 1s of GO/TiO_2 (as shown in Fig. 3B), the oxygenated functional groups are significantly reduced in rGO/TiO_2/AuNW, indicating the room temperature reduction of GO by OA. This is also evident from XRD analysis that shows a reduction in the basal spacing resulting from the reduction of GO (Fig. S1).[45] Additionally, similar GO reduction (without TiO_2) was observed (Fig. S8) under incubation of GO in Au nanowire growth solution suggesting simultaneous room temperature reduction of GO and Au with OA. Therefore, it can be deduced that the room temperature reduction of GO is facilitated by the amine.

In particular, based on mechanisms proposed in the literature, nucleophilic substitution between amine and GO leads to deoxygenation and reduction of GO.[40] Interestingly, a shift of Au binding energy towards lower values was observed for TiO_2 (Fig. S9) and rGO/TiO_2 (Fig. 3C) supported ultrathin Au nanowires as compared to the Au nanowires on bare GO (Fig. 3D). We propose that electron transfer from TiO_2 to Au contributes to the observed shift, leading to electron accumulation in the Au wire.[12] From the relative position of the Au work function, intrinsic defect states (F-center electron) and conduction band of TiO_2,[46] an electron from F-center of TiO_2 can migrate to Au contributing to the reduction in the binding energy as observed by XPS. On the contrary, no shift in Au 4f was observed for rGO/AuNW (Fig. 3D) validating the hypothesis of electron transfer from TiO_2 to Au.

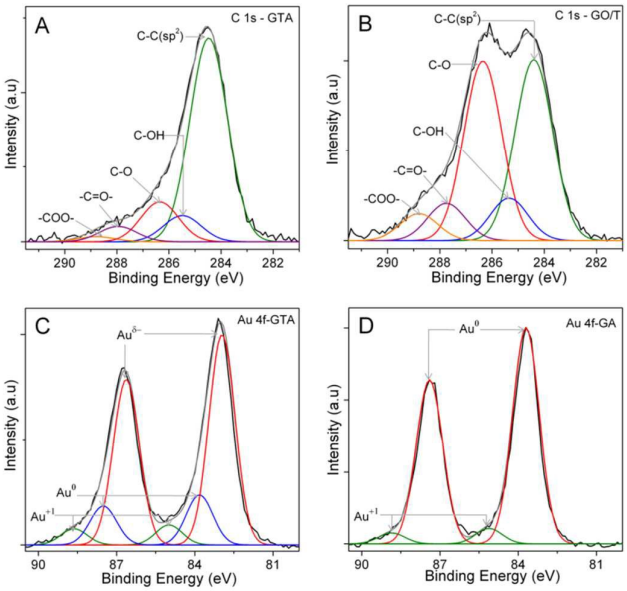

Fig. 3 XPS spectra of as-synthesized samples. High-resolution C 1s spectra of GO/TiO_2 (A) after and (B) before growth of AuNW. The least-square fitted peaks reveals that the contributions from –C-O, C-OH –C=O and –COO- groups decreased after nanowire growth, indicating reduction of GO. (C) Deconvoluted Au 4f of rGO/TiO_2/AuNW showing the presence of $Au^{\delta-}$ species possibly due to electron transfer from TiO_2 to Au. (D) No $Au^{\delta-}$ was observed in case of rGO/Au nanowires. Legend representation: GO-graphitic oxide, G- rGO, T- TiO_2 and A- Au.

Support-dependent electrocatalytic activity

We carried out alcohol oxidation reaction to test the electrochemical properties of the ternary and binary hybrids. On the basis of both theoretical calculation and experimental observations, electrocatalytic oxidation of alcohols requires OH^- adsorption or pre-oxidation species on the catalyst gold surface.[47, 48] These species act as an oxidant, leading to a significant reduction in the activation energies for electrocatalytic alcohol oxidation. Indeed, several studies have validated that the appearance of redox features are mandatory for alcohol oxidation on gold surface.[30, 47, 49]

Therefore, we have initially evaluated the electrodes for the redox features in 1 M NaOH at a scan rate of 40 mV/s (Fig. 4A).

Cyclic voltammograms of rGO/TiO_2/AuNW exhibit a broad peak around 0.3 V that corresponds to partial oxidation of Au surface accompanied by the reduction of formed oxide at -0.01 V in the reverse scan. Based on the IHOAM model,[47] the observed characteristic gold redox features, suggests that the ternary hybrid could be active towards ethanol oxidation. We note that the inherent inertness of Au due to deep d-band position[6] towards chemisorption of oxygenated species is by-passed here with the presence of TiO_2 in the support. To validate the role of TiO_2, rGO/Au nanowires with comparable ratio of Au to carbon was employed for comparison. The voltammograms in this case are featureless while cycling up to 0.6 V as shown in Fig. 4A. Moreover, when repeatedly scanning between -0.3 V to 0.6 V for multiple cycles, there is no reduction peak of Au oxide in the reverse scan indicating that absence of Au redox reactions in this case. However, increasing the cycling potential range to +1 V for a few cycles leads to redox features as manifested in the form oxidation and reduction peaks at 0.3 V and -0.01 V, respectively. Once the redox features start to appear, they remain even when the subsequent cycling range is reduced back to 0.6 V. This observation implies that high positive potential is initially needed to possibly pre-activate the Au surface.

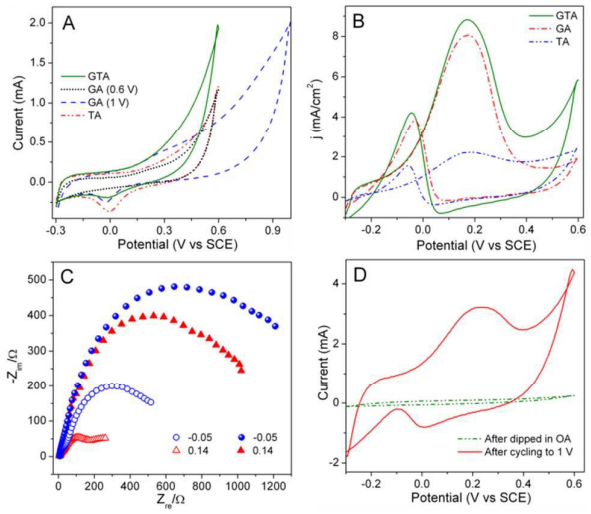

Fig. 4 (A) Cyclic voltammograms in 1 M NaOH of rGO/TiO_2/AuNW (GTA), rGO/AuNW (GA), TiO_2/AuNW (TA) electrodes. Nanowires without TiO_2 nanoparticles (GA) needs high positive potential to exhibit characteristics Au redox features. (B) CVs of supported nanowires measured in 1 M NaOH containing 1.5 M ethanol at a scan rate of 40 mV/s showing support-dependent activity. The presence of conducting rGO support leads to a higher oxidation current. (C) Nyquist plot at different applied potentials showing that charge transfer resistances are relatively low for AuNW grown on conducting support in 1.5 M ethanol and 1 M NaOH. Hollow and solid symbols represent GA and TA, respectively. (D) CVs measured in 1 M NaOH containing 1.5 M ethanol for pre-activated GA electrode showing negligible EOX current after dipping the electrode in hexane containing oleylamine. After cycling to high positive potential for several cycles, the same electrode exhibited activity. Legend representation: G-rGO, T-TiO_2 and A-Au.

To obtain further insights into the role played by TiO_2 in the ternary catalyst, we prepared TiO_2/AuNW hybrids. The CV curve of TiO_2/AuNW electrode was recorded as shown in Fig. 4A which shows oxidation and reduction features of Au at much lower potential values similar to that seen in rGO/TiO_2/AuNW. We rationalize that the observed redox feature is possibly due to the migration of electrons from F-center of TiO_2 to Au [46] that could be beneficial for adsorption of hydroxyl groups. This is also evident from the Au 4f spectra in the samples containing TiO_2 (Fig. 3C, for instance). This implies that TiO_2 has an electronic effect on Au that drives the formation of incipient hydrous oxide at low potentials that can act as a mediator for ethanol oxidation (EOX).

In the case of rGO/AuNW, active Au redox surfaces are only obtained after higher positive potential scan, which can be considered to be a kind of activation in order to form oxygenated species on the Au surface. The presence of oleylamine bound to the nanowires surface hampers the adsorption of OH^-. The amine forms a complex with Au in basic solution that can be oxidized only at high positive potential.[47] Also, the inherent hydrophobic nature of oleylamine prevents the effective adsorption of OH^- from the electrolyte.[50] The origin of the activation at a higher potential is possibly due to the oxidation of the undesirable oleylamine complex that leads to the appearance of the redox features in the following cycles.[47, 30]

High resolution XPS was used to investigate the chemical change on the rGO/AuNW electrodes scanned to different final positive potentials. The O 1s XPS spectrum of rGO/AuNW dipped in the electrolyte (1 M NaOH and 1.5 M ethanol solution) before any electrochemical cycling is displayed in Fig. S10. In this case, the oxygen spectrum displays a slightly higher content of -C=O species as compared to the as-synthesized hybrid nanowires. The oxygen containing amide (carbonyl) group, dramatically increased by scanning the electrode to 0.6 V. Further increase in the potential to 1 V resulted in a decrease in the amide groups while the relative ratios of the other oxygen species are similar to the as-synthesized hybrid. The change in the amount of the amide after scanning to 1 V accounts for the very different catalytic behavior and redox process of the hybrid (Fig. S10). The presence of the amide may block OH^- adsorption and impede the redox process of Au. The oxidation of the amide by sweeping to high positive potential allows the OH^- adsorption on Au and is the key mechanism for the activation of the hybrid.

Ethanol oxidation (EOX) efficiencies of the hybrids were investigated in an alkaline medium. The ethanol oxidation peak on rGO/TiO_2/AuNW reaches a maximum at 0.17 V (Fig. 4B) accompanied by a peak in the reverse scan at -0.04 V that corresponds to the removal of carbonaceous species that are formed due to the incomplete oxidation in the forward scan.[51] As shown in Fig. 4B, significant differences in the oxidation current density between the ternary and binary (TA) catalysts are observed highlighting the role of supports. Compared with TiO_2/AuNW, the rGO-supported AuNW showed remarkably higher oxidation current, which is directly related to the improvement in the conductivity. To further validate this, we carried out electrochemical impedance spectroscopy (EIS) to determine the interfacial charge resistance influenced by the

different supports during ethanol oxidation. Fig. 4C shows the representative Nyquist complex plane impedance spectra at different applied potentials; charge transfer resistance is notably lower for rGO-supported nanowires (275 Ω for rGO/TiO_2/AuNW as compared to 1050 Ω for TiO_2/AuNW). This result indicates the beneficial role of rGO integration in the catalyst as confirmed from the CV results as well. The absence of ethanol oxidation peak with just rGO/TiO_2 support validates that the observed electrocatalytic activity stems from the Au nanowires (Fig. S11). Thus both TiO_2 nanoparticles and rGO add their specific beneficial effect to the AuNW, leading to a superior ternary system. Further tests showed that the activity of rGO/AuNW (without TiO_2 nanoparticles) was negligible without activation at a high positive potential. The activated samples show a dramatic reduction in the current density after dipping the electrode in hexane containing oleylamine further confirming the detrimental role of OA for electrooxidation (Fig. 4D). Upon potential cycling to 1 V for several sweeps, the catalyst exhibited EOX oxidation activity (Fig. 4D). We note that there is no morphological change in the supported wires that was observed even after high potential scan in contrast to ultrathin Au nanowires that were drop-cast on the substrate (Fig. 5). This clearly indicates the beneficial role of the direct growth of the wires on the substrate that leads to good binding and higher stability of the nanowires.

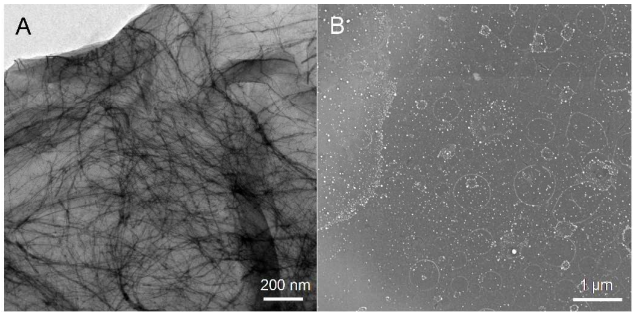

Fig. 5 TEM and SEM micrographs of rGO/AuNW (A) and bare AuNW (B) recorded after cycling to 1 V in 1 M NaOH containing 1.5 M ethanol indicating that supported nanowires are stable during electrocatalysis reactions while drop-cast nanowires disintegrate into nanoparticles.

The impact of Au morphology (wire) on electrocatalytic activity was studied; the activity of rGO/TiO_2/Au nanoparticles, and TiO_2/Au nanoparticles was compared with the observed activity of the supported nanowire hybrids. The supported nanoparticles displayed current density that was atleast 50% smaller than that of nanowire hybrids as shown in Fig. 6A. Moreover, as was the case with the nanowire hybrids, it is observed that the rGO-supported nanoparticles possessed better activity compared to the nanoparticle hybrids without rGO.

The long-term stability, the minimization of cross-over and poisoning effects are critical for the use of the hybrids for real applications. The ternary rGO/TiO_2/AuNW exhibited good stability in ethanol oxidation over multiple cycles with a negligible drop in activity over 100 cycles of test (Fig. S12). It should be pointed out that our method to grow ultrathin nanowires on support overcomes the inherent instability of wires in polar medium like ethanol.[29] One of the other key drawbacks in EOX is the dramatic decrease in the kinetics of oxidation owing to the presence of intermediates like CO that compete with ethanol for adsorption. An experiment was conducted to evaluate the electrocatalytic oxidation of CO by means of CO stripping test (Fig. S13). Most of the previous studies suggest that the presence of TiO_2 nanoparticles would increase OH^- species near the vicinity of the Au surface, which leads to an increased CO oxidation activity via bifunctional mechanism.[52, 53] This is apparently not the case in our present systems, as our CO stripping experiments (Fig. S13) clearly revealed that supported Au nanowires exhibited less current density when compared to reported Au nanoparticles.[54, 55] This observation coupled with the fact that the EOX current does not decrease implies that CO adsorption does not poison the catalyst in the present case.

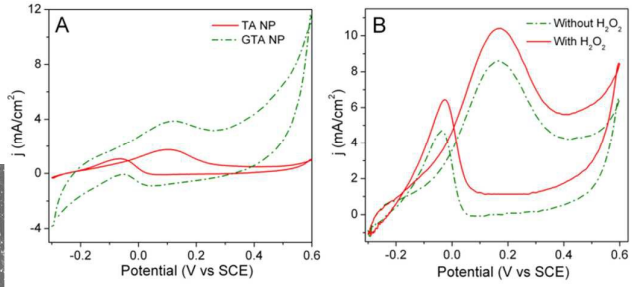

Fig. 6 (A) CVs of rGO/TiO_2/Au nanoparticles (GTA NP) and TiO_2/Au nanoparticles (TA NP) in 1 M NaOH containing 1.5 M ethanol at the scan rate of 40 mV/s showing that the current density that are significantly lower as compared with nanowire hybrids. (B) Tolerance test to avoid cross-over effects. CV curves of rGO/AuNW recorded in 1 M NaOH containing 1.5 M ethanol in the absence (a) and presence (b) of H_2O_2 (0.4 M).

The cross-over effect of supported nanowires with respect to H_2O_2 oxidant was assessed through CV measurements. Membrane fuel cells employing H_2O_2 as oxidant are received increasing attention because of their high theoretical voltages. It is well-documented that H_2O_2 can oxidize on Au surface through a free-radical chain reaction.[56] Considering the fact that interaction of H_2O_2 with AuNW is likely to decrease ethanol oxidation current in the presence of H_2O_2, we examined the crossover effects of H_2O_2 during ethanol oxidation reaction. Surprisingly, we observed an increase in ethanol oxidation current for rGO/AuNW in the presence of H_2O_2[57] (Fig. 6B), coupled with existence of oxidation peak of H_2O_2 at -0.11 V in the forward scan. This result demonstrates that nanowire hybrid possesses enhanced EOX with negligible poisoning effects, which is crucial for developing direct ethanol-hydrogen peroxide fuel cells.

Photo-assisted electrocatalytic activities

Considering that TiO_2 is a traditional photocatalyst, we coupled the effect of solar light irradiation on TiO_2 with the electrocatalytic activity of ultrathin nanowire. The effect of irradiation on the electrooxidation current using TiO_2 was investigated. A significant increase in the current with solar light illumination (as shown in Fig. 7A), indicates that the photogenerated charge carriers are consumed for ethanol oxidation. Furthermore, as anticipated, a higher oxidation current was observed for TiO_2/AuNW under illumination as shown in Fig. 7B. Importantly, the magnitude of the photocurrent density is higher than the algebraic sum of ethanol photo-oxidation current of TiO_2 and electrocatalytic current of TiO_2/AuNW. It is well documented that under illumination electron and hole pairs are generated in TiO_2 (reaction 1)

$$TiO_2 + h\nu \rightarrow e_{CB}^- + h_{VB}^+ \quad (1)$$

$$C_2H_5OH + \bullet OH\ (OH + h^+) \rightarrow \bullet CH(OH)CH_3 + H_2O \quad (2)$$

$$\bullet CH(OH)CH_3 + 11 \bullet OH \rightarrow 2\ CO_2 + 8\ H_2O \quad (3)$$

Since the electron affinity of TiO_2 is lower than the Fermi level of Au, photo-excited electron transfer from conduction band of TiO_2 to Au is energetically favorable (Scheme 1)[58] and an effective charge separation is achieved. The photo-generated holes promote further oxidation of ethanol via hydroxyl radicals (reaction 2).[59] Another frequently occurring phenomenon in alcohol photo-oxidation is that of 'current doubling' (reaction 3) whereby oxidation of α-hydroxyethyl intermediate radical proceeds with constant injection of electron to conduction band of TiO_2.[60] These electrons along with F-center electrons stimulate the adsorption of hydroxyl group on the Au surface (Scheme 1) that enhances the electrocatalytic activity of nanowires. Thus, the enhanced current density is attributed to synergetic effect of photo-assisted electrocatalytic activity of nanowires.

The introduction of rGO support significantly increases the generated photocurrent throughout the potential region (Fig.7B). The higher photo-electrocatalytic activity of ternary rGO/TiO_2/AuNW observed in this study can be attributed to the enhancement of charge separation in the presence of rGO that extends the lifetime of the active species[61,62] and a possible photosensitizing effect of rGO on TiO_2 that can increase the photon flux by absorbing a wide range of the light spectrum[63] (Fig. S14). Thus, the TiO_2 and rGO add their specific benefits to AuNW, leading to a superior performance.

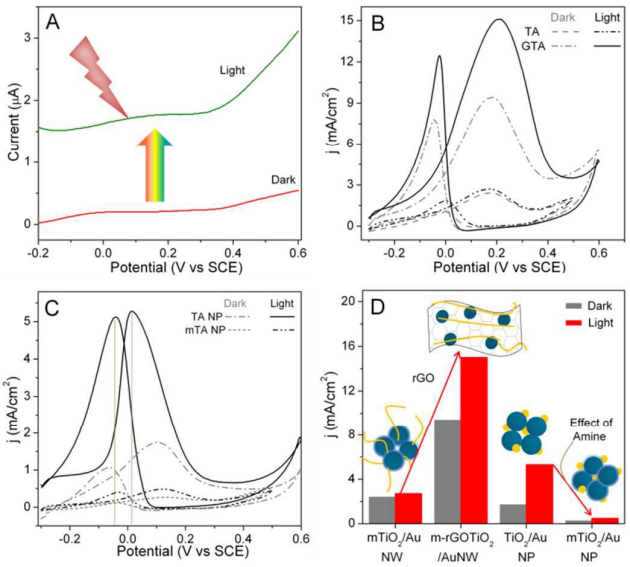

Fig. 7 CVs of synthesized catalyst recorded in 1 M NaOH containing 1.5 M ethanol at a scan rate of 40 mV/s. TiO_2 electrode showing (A) significant increase in the electrooxidation current under irradiation using a xenon lamp. (B) rGO/TiO_2/AuNW exhibits higher photo-assisted electroactivity than TiO_2/AuNW showing the influence of the conducting GO substrate. TA and GTA indicate TiO_2/AuNW and rGO/TiO_2/AuNW, respectively. (C) Au nanoparticles nucleated on unmodified TiO_2 (TA NP) displays marked enhancement in photocurrent with considerable potential shift while Au nanoparticles nucleated on oleylamine modified TiO_2 (mTA NP) exhibit low photoactivity. (D) Summary of the electro and photo activity of the hybrids evaluated by CV measurements. Amine effect was nullified by incorporated rGO, which facilitates the fast electron transfer.

To examine the role of morphology of Au on photoelectrocatalytic activity, we compare the activity of TiO_2/AuNW with TiO_2/Au nanoparticles. The Au nanoparticle hybrid was synthesized without surface modification of TiO_2 with amine, unlike the growth of ultrathin Au nanowires on amine-modified TiO_2. TEM micrographs of supported Au nanoparticles are shown in Fig. S15. The electrocatalytic oxidation current density of TiO_2/Au nanoparticles is only 1.7 mA/cm^2, but under illumination shows a 3-fold increase (Fig. 7C) and is higher than the photoresponse of nanowire hybrids. In addition, the characteristic oxidation EOX peak for TiO_2/Au nanoparticles was shifted to much lower potential with light as marked in the Fig. 7C, the smallest potential reported so far.[51] Similarly, the oxidation of intermediate carbonates also occurred at higher positive potential in the reverse scan. We hypothesize the observed inferior photoresponse in the case of hybrid nanowire, may be due to the modification of the TiO_2 support with the amine. Indeed, investigations have demonstrated that the charge injection between metal oxide and metal is directly affected by the presence of interface dipoles induced by ligands like amine.[64, 65]

To inspect the electronic interaction between TiO_2 and amine, we nucleated Au nanoparticles on an amine-modified TiO_2 similar to that used for nanowire growth (for detailed synthesis steps, please see Experimental Section) and employed this as the photoanode (Fig. 7C). The electro and

photo-catalytic activity towards ethanol oxidation was dramatically reduced as compared to unmodified TiO_2/Au nanoparticles (as shown in Fig. 7D). In addition, this is also reflected in I-V measurements, which displays drastic decrease in photo and electrocurrent of TiO_2 after amine modification (as shown in Fig. 8A). Further, the amine grafting was verified with XPS analysis; deconvoluted N 1s spectra of modified TiO_2 displays peaks at 398.8 and 400.3 eV (Fig. 8B), which are associated with nitrogen atoms in oleylamine and oleylammonium cation.[41] These findings highlight that amine-grafted TiO_2 reduce the electro and photoconductivity unlike the increase that happens in the case of ZnO nanorods.[30] The above results highlight that while amine modification of TiO_2 is essential to grow ultrathin AuNW, the presence of the amine reduces the overall photoresponse of the hybrid.

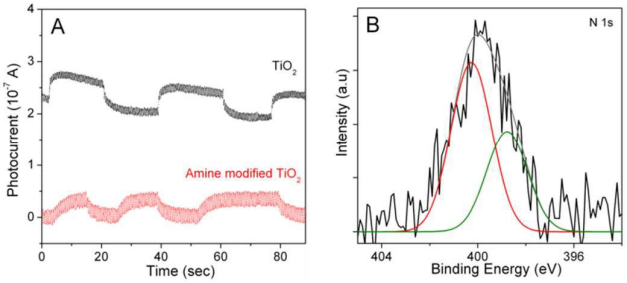

Fig. 8 (A) Photocurrent of TiO_2 with and without amine modification upon solar illumination (Xenon lamp), amine grafting deactivates the electro and photo conductivities of TiO_2. (B) Deconvoluted N 1s spectra of oleylamine modified TiO_2, showing the existence of nitrogen species.

In our earlier report, we have shown that amine modifies the surface of ZnO nanorods by passivating the surface dangling bonds that in turn enhances the photo-current and catalytic activity.[30] However, the amine has a detrimental effect on the photocurrent and catalytic activity of TiO_2. The above result suggests that the charge transfer scenario is different in ZnO nanorods and TiO_2 nanoparticles after amine modification. Based on the literature reports for the effects of surface modification on metal oxides, it appears that long chain ligand grafting leads to two counter effects.[66] Firstly, the linked ligands can permanently passivate the surface defect/shield the recombination centers, resulting in an enhancement in the photoactivity by suppressing non-radiative recombination.[67] The second effect is a dipole effect wherein long chain molecules at the oxide surface create fields that hinder the charge transfer process at the interface. The former effect dominates in 1-D ZnO because single crystalline long nanorods are known for efficient charge transporter, so it overwhelms the later effect.[68, 69] However, in the present case, the TiO_2 nanoparticles are not interconnected and thus the interfacial charge transfer is deteriorated. As complied in Fig. 7D, the comparative analysis of photo and electrocatalytic activity between the different binary and ternary hybrids provides interesting information. The effect of amine is not so pronounced in the ternary hybrid when rGO is present, as shown in Fig. 7B. This clearly indicates that the presence of rGO opens up path for the transfer of photogenerated charge carriers either to electrolyte or Au surface through rGO (as shown in Scheme 1). Considering the work function levels, the presence of rGO suggests that there would be a dynamic electron (photogenerated) transfer from TiO_2 to Au,[20] leading to net separation of photogenerated charge carriers as shown in Scheme 1. These findings highlight that direct interference of rGO, involved in the interfacial charge transport is likely to boost the photoassisted electrocatalytic performance (as shown in the Scheme 1).

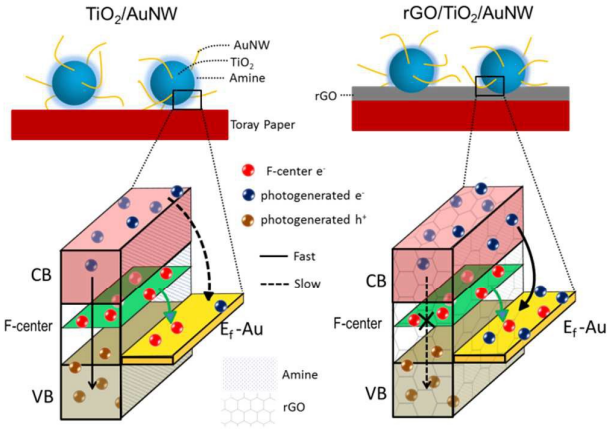

Scheme 1. Illustration depicts the effect of amine and rGO on interfacial photo-induced charge transfer in both binary (TiO_2/AuNW) and ternary system (rGO/TiO_2/AuNW).

Conclusions

In conclusion, we have developed a new type of multidimensional 0-D TiO_2, 1-D AuNW and 2-D rGO ternary hybrid electrocatalyst by controlled growth of ultrathin Au nanowires on rGO sheet in contact with TiO_2 nanoparticles. The amine molecules involved in the reaction not only assist the dense growth of ultrathin Au nanowires on TiO_2 /GO sheets but also stimulate the room temperature reduction of GO. Our investigation reveals that the electrochemical activity rests on the synergy between integral constituents of the catalyst. Specifically, the change in Au electronic structure by the migrated electrons from TiO_2 favors generation of oxygenated species at less positive potential that promotes the alcohol oxidation. Systematic study of support reveals that rGO reduces the charge transfer resistance of ternary electrode and also stabilizes the nanowires during performance. In addition to the stability, inherent optoelectronic properties of the support synergistically enhance the performances of nanowires. The incorporation of rGO is also mandatory to nullify the negative effect of amine on TiO_2 especially during photo-assisted electrocatalytic oxidation. The above-mentioned insights clearly point the direction for synthesizing hybrids with enhanced performance for various applications beyond fuel cell applications.

Experimental

Synthesis of GO/TiO_2

The graphene oxide (GO) was first prepared based on the modified Hummer's method.[22] For the microwave synthesis of GO/TiO_2 hybrid, 10 mg of GO was sonicated in 30 mL of de-ionized water for 20 min to achieve a homogeneous dispersion. Titanyl nitrate ($TiO(NO_3)_2$) which was prepared by dissolving titanium isopropoxide (250 µL) in a few drops of concentrated nitric acid was added to the above GO dispersion, followed by addition of 1 M NaOH (1 mL). Finally, the suspension was sonicated for 5 min and then subjected to microwave (2.45 GHz, 300 W) for 3 min. After the reaction, the suspension was cooled down to room temperature in ambient conditions. The products were centrifuged and washed with distilled water for several times, finally dried at 100 ^{0}C.

Formation of supported nanowire hybrids

To obtain ternary rGO/TiO_2/AuNW, the above synthesized GO/TiO_2 was introduced into the gold nanowires growth solution (containing appropriate amounts of $HAuCl_4$ (3 mg), oleylamine (100 µL) and tetraisopropylsilane (150 µL) in 2.5 mL of hexane).[38] The mixture was sonicated for 1 min and then incubated for 6 h at room temperature. The end product was cleaned with hexane and ethanol to removal undesired loosely bound ultrathin nanowires along with unreacted precursors, if present.

rGO/AuNW was prepared by adding GO into gold nanowires growth solution and left undisturbed for 24 h. The obtained product was washed with hexane and ethanol, to remove unreacted reagents. As-synthesized rGO/AuNW were stored in hexane for future characterization and electrochemical tests.

To synthesize TiO_2/AuNW, initially anatase TiO_2 nanoparticles were prepared by sol-gel combustion method based on our earlier report.[70] To grow ultrathin AuNW on TiO_2, solid state mixing was adopted to modify the surface of TiO_2 with oleylamine. 50 µL of oleylamine was mixed with TiO_2 (100 mg) using mortar and pestle, the obtained product was cleaned with hexane and ethanol mixture to remove unbound oleylamine.[30] Finally, the amine modified TiO_2 was dried and introduced into the Au nanowires growth solution. TEM micrographs revealed that without surface modification of TiO_2 leads to primarily larger Au nanoparticles, which implies that amine modification is required for the growth of nanowires on TiO_2 substrate.

Synthesis of nanoparticle hybrid

30 mg of TiO_2 was sonicated for 15 min in 30 mL of water to obtain homogeneous dispersion and 5 mg of $HAuCl_4$ was added. Then the reaction mixture was subjected to microwave for subjected to microwave (2.45 GHz, 800 W) for 3 min.[71] The resulting products were washed several times with distilled water and then dried at 100 ^{0}C for further use. Under identical conditions instead of TiO_2, GO/TiO_2 was used to obtain rGO/TiO_2/Au nanoparticles.

Amine grafted TiO_2 (30 mg) was taken in 5 mL of ethanol, 5 mg of $HAuCl_4$ was added. This was followed by drop-wise addition of sodium borohydride (dissolved in ethanol) to the above solution under mild stirring. Then the solution was centrifuged and washed several times with ethanol.

Characterizations

The microstructure of the synthesized samples were characterized by transmission electron microscopy (TEM, FEI Technai T20) operated at accelerating voltages of 200 kV. The samples were dispersed in ethanol and drop casted on carbon coated Cu-grids. The scanning electron microscopy (SEM) images were acquired using field emission SEM, Ultra55 Carl Zeiss. XRD was performed on a Phillips X'pert diffractometer using Cu Kα radiation. The chemical analysis were analyzed by using X-ray photoelectron spectroscopy (XPS, Axis Ultra) with monochromatic source of Al Kα radiation and graphitic carbon peak at 284.5 eV was used for charge correction.

Photoelectrochemical measurements

The electrochemical properties were examined by cyclic voltammetry (CV) as well as with CO stripping voltammetry using three electrode cell. A platinum foil was used as a counter electrode and saturated calomel electrode (SCE) as reference. The working electrodes were prepared by drop casting known concentration of hexane stored supported nanowires on Toray paper. The prepared electrodes were dried overnight at room temperatures before electrocatalytic tests. All the experiments were carried out at room temperatures in NaOH (1 M) either with or without ethanol as electrolyte solution. CVs of the electrodes were measured with and without light irradiation. A Xenon lamp of 100 W was used as light source. For CO stripping experiments, the electrolyte solution was saturated with CO (99.99%, CHEMIX gases-Bangalore, India) by bubbling CO for 30 min through the solution. Subsequently, the electrodes were scanned to obtain the corresponding CO stripping CVs. All the experiments were conducted at room temperature and performed by potentiostat (PG26250, Techno Science Instrument).

Electrochemical impedance spectroscopy (EIS) measurements

EIS measurements were carried out using three electrode system, CHI 660D electrochemical workstation. The spectra were collected using an AC signal of 10 mV from 100 kHz to 10 MHz.

Photoconductivity measurements

Photocurrent I-V measurements, were performed using Class 3A solar simulator (Oriel Sol 3A) comprising a Xenon lamp 450 W, with a 1.5 air mass filter and a Keithley (2420 model) source meter. An ITO coated glass with a non-conducting gap (50 µm) was adopted as an electrode. The samples were dispersed in ethanol and drop casted on the gap between ITO contacts.

Acknowledgements

We thank Prof. Praveen C. Ramamurthy for impedance measurements facility. The Tecnai T20 is a part of Advanced facility for Microscopy and Microanalysis at IISc. The XPS and solar simulator are part of MNCF, CeNSE, IISc. NR acknowledges financial support from the TUE and Swarnajayanti Fellowship from DST.

Notes and references

1. M. Haruta, *Nature*, 2005, **437**, 1098-1099.
2. A. S. K. Hashmi, *Science*, 2012, **338**, 1434-1434.
3. N. Marković, R. Adić and V. Vešović, *J. Electroanal. Chem. Interfacial Electrochem.*, 1984, **165**, 121-133.
4. C. N. Brodsky, A. P. Young, K. C. Ng, C.-H. Kuo and C.-K. Tsung, *ACS nano*, 2014, **8**, 9368-9378.
5. Z.-P. Liu, P. Hu and A. Alavi, *J. Am. Chem. Soc.*, 2002, **124**, 14770-14779.
6. B. Hammer and J. Norskov, *Nature*, 1995, **376**, 238-240.
7. A. Kowal, M. Li, M. Shao, K. Sasaki, M. Vukmirovic, J. Zhang, N. Marinkovic, P. Liu, A. Frenkel and R. Adzic, *Nat. Mater.*, 2009, **8**, 325-330.
8. C. Zhu, S. Guo and S. Dong, *Adv. Mater.*, 2012, **24**, 2326-2331.
9. C. Koenigsmann, E. Sutter, R. R. Adzic and S. S. Wong, *J. Phys. Chem. C*, 2012, **116**, 15297-15306.
10. S. J. Yoo, T.-Y. Jeon, K.-S. Lee, K.-W. Park and Y.-E. Sung, *Chem. Commun.*, 2010, **46**, 794-796.
11. S.-Y. Huang, P. Ganesan, S. Park and B. N. Popov, *J. Am. Chem. Soc.*, 2009, **131**, 13898-13899.
12. S. Arrii, F. Morfin, A. Renouprez and J. Rousset, *J. Am. Chem. Soc.*, 2004, **126**, 1199-1205.
13. J. Mann, N. Yao and A. B. Bocarsly, *Langmuir*, 2006, **22**, 10432-10436.
14. M. Haruta, *Catal. Today*, 1997, **36**, 153-166.
15. K. Drew, G. Girishkumar, K. Vinodgopal and P. V. Kamat, *J. Phys. Chem. B*, 2005, **109**, 11851-11857.
16. R. Kou, Y. Shao, D. Mei, Z. Nie, D. Wang, C. Wang, V. V. Viswanathan, S. Park, I. A. Aksay and Y. Lin, *J. Am. Chem. Soc.*, 2011, **133**, 2541-2547.
17. Z.-Z. Jiang, Z.-B. Wang, Y.-Y. Chu, D.-M. Gu and G.-P. Yin, *Energy Environ. Sci.*, 2011, **4**, 2558-2566.
18. H. Huang, S. Yang, R. Vajtai, X. Wang and P. M. Ajayan, *Adv. Mater.*, 2014, **26**, 5160-5165.
19. S. Shanmugam and A. Gedanken, *Small*, 2007, **3**, 1189-1193.
20. P. V. Kamat, *J. Phys. Chem. Lett.*, 2010, **1**, 520-527.
21. G. Goncalves, P. A. Marques, C. M. Granadeiro, H. I. Nogueira, M. Singh and J. Gracio, *Chem. Mater.*, 2009, **21**, 4796-4802.
22. C. Nethravathi, E. Anumol, M. Rajamathi and N. Ravishankar, *Nanoscale*, 2011, **3**, 569-571.
23. Y. H. Ng, I. V. Lightcap, K. Goodwin, M. Matsumura and P. V. Kamat, *J. Phys. Chem. Lett.*, 2010, **1**, 2222-2227.
24. Y. T. Liang, B. K. Vijayan, O. Lyandres, K. A. Gray and M. C. Hersam, *J. Phys. Chem. Lett.*, 2012, **3**, 1760-1765.
25. I. V. Lightcap, T. H. Kosel and P. V. Kamat, *Nano Lett.*, 2010, **10**, 577-583.
26. A. Roy, S. Kundu, K. Müller, A. Rosenauer, S. Singh, P. Pant, M. P. Gururajan, P. Kumar, J. Weissmüller and A. K. Singh, *Nano Lett.*, 2014, **14**, 4859-4866.
27. C. Koenigsmann, A. C. Santulli, K. Gong, M. B. Vukmirovic, W.-p. Zhou, E. Sutter, S. S. Wong and R. R. Adzic, *J. Am. Chem. Soc.*, 2011, **133**, 9783-9795.
28. C. Koenigsmann, W.-p. Zhou, R. R. Adzic, E. Sutter and S. S. Wong, *Nano Lett.*, 2010, **10**, 2806-2811.
29. E. Koposova, A. Kisner, G. Shumilova, Y. Ermolenko, A. Offenhäusser and Y. Mourzina, *J. Phys. Chem. C*, 2013, **117**, 13944-13951.
30. A. Leelavathi, G. Madras and N. Ravishankar, *J. Am. Chem. Soc.*, 2014, **136**, 14445-14455.
31. A. Halder and N. Ravishankar, *Adv. Mater.*, 2007, **19**, 1854-1858.
32. P. Kundu, A. Halder, B. Viswanath, D. Kundu, G. Ramanath and N. Ravishankar, *J. Am. Chem. Soc.*, 2009, **132**, 20-21.
33. A. Halder, P. Kundu, B. Viswanath and N. Ravishankar, *J. Mater. Chem.*, 2010, **20**, 4763-4772.
34. P. Kundu, C. Nethravathi, P. A. Deshpande, M. Rajamathi, G. Madras and N. Ravishankar, *Chem. Mater.*, 2011, **23**, 2772-2780.
35. T. Ohsaka, F. Izumi and Y. Fujiki, *J. Raman Spectrosc.*, 1978, **7**, 321-324.
36. G. Williams, B. Seger and P. V. Kamat, *ACS nano*, 2008, **2**, 1487-1491.
37. X. Liu, L. Pan, T. Lv, G. Zhu, T. Lu, Z. Sun and C. Sun, *RSC Adv.*, 2011, **1**, 1245-1249.
38. S. Kundu, A. Leelavathi, G. Madras and N. Ravishankar, *Langmuir*, 2014, **30**, 12690-12695.
39. K. Yang, S. Liang, L. Zou, L. Huang, C. Park, L. Zhu, J. Fang, Q. Fu and H. Wang, *Langmuir*, 2012, **28**, 2904-2908.
40. C. K. Chua and M. Pumera, *Chem. Soc. Rev.*, 2014, **43**, 291-312.
41. A. Loubat, M. Impéror-Clerc, B. Pansu, F. Meneau, B. Raquet, G. Viau and L.-M. Lacroix, *Langmuir*, 2014, **30**, 4005-4012.
42. Y. Li, Y. Zhao, H. Cheng, Y. Hu, G. Shi, L. Dai and L. Qu, *J. Am. Chem. Soc.*, 2011, **134**, 15-18.
43. R. Rozada, J. I. Paredes, S. Villar-Rodil, A. Martínez-Alonso and J. M. Tascón, *Nano Res.*, 2013, 1-18.
44. Z.-J. Fan, W. Kai, J. Yan, T. Wei, L.-J. Zhi, J. Feng, Y.-m. Ren, L.-P. Song and F. Wei, *ACS nano*, 2010, **5**, 191-198.
45. I. K. Moon, J. Lee, R. S. Ruoff and H. Lee, *Nat. Commun.*, 2010, **1**, 73.
46. Z. Yan, S. Chinta, A. A. Mohamed, J. P. Fackler and D. W. Goodman, *J. Am. Chem. Soc.*, 2005, **127**, 1604-1605.
47. L. Burke and P. Nugent, *Gold Bull.*, 1998, **31**, 39-50.
48. R. De Lima and H. Varela, *Gold Bull.*, 2008, **41**, 15-22.
49. B. N. Zope, D. D. Hibbitts, M. Neurock and R. J. Davis, *Science*, 2010, **330**, 74-78.
50. J. Xu, Y. Zhu, J. Zhu and W. Jiang, *Nanoscale*, 2013, **5**, 6344-6349.
51. J. Huang, X. Han, D. Wang, D. Liu and T. You, *ACS Appl. Mater. Interfaces*, 2013, **5**, 9148-9154.
52. G. M. Veith, A. R. Lupini and N. J. Dudney, *J. Phys. Chem. C*, 2008, **113**, 269-280.
53. J. Saavedra, H. A. Doan, C. J. Pursell, L. C. Grabow and B. D. Chandler, *Science*, 2014, **345**, 1599-1602.
54. P. Diao, D. Zhang, M. Guo and Q. Zhang, *J. Catal.*, 2007, **250**, 247-253.
55. T. E. Shubina, C. Hartnig and M. T. Koper, *Phys. Chem. Chem. Phys.*, 2004, **6**, 4215-4221.
56. J. Kim and A. A. Gewirth, *J. Phys. Chem. B*, 2006, **110**, 2565-2571.

57. Y. Kwon, S. J. Raaijman and M. Koper, *ChemCatChem*, 2014, **6**, 79-81.
58. M. Jakob, H. Levanon and P. V. Kamat, *Nano Lett.*, 2003, **3**, 353-358.
59. V. Subramanian, E. E. Wolf and P. V. Kamat, *J. Am. Chem. Soc.*, 2004, **126**, 4943-4950.
60. Y. Harima and S. R. Morrison, *J. Electroanal. Chem. Interfacial Electrochem.*, 1987, **220**, 173-177.
61. A. L. Linsebigler, G. Lu and J. T. Yates Jr, *Chem. Rev.*, 1995, **95**, 735-758.
62. Z. Zhang, C.-C. Wang, R. Zakaria and J. Y. Ying, *J. Phys. Chem. B*, 1998, **102**, 10871-10878.
63. P. Song, X. Zhang, M. Sun, X. Cui and Y. Lin, *Nanoscale*, 2012, **4**, 1800-1804.
64. N. R. Neale, N. Kopidakis, J. van de Lagemaat, M. Grätzel and A. J. Frank, *J. Phys. Chem. B*, 2005, **109**, 23183-23189.
65. X. Crispin, V. Geskin, A. Crispin, J. Cornil, R. Lazzaroni, W. R. Salaneck and J.-L. Bredas, *J. Am. Chem. Soc.*, 2002, **124**, 8131-8141.
66. A. J. Morris and G. J. Meyer, *J. Phys. Chem. C*, 2008, **112**, 18224-18231.
67. J. W. Soares, J. E. Whitten, D. W. Oblas and D. M. Steeves, *Langmuir*, 2008, **24**, 371-374.
68. X. Pan, Y. Zhao, S. Liu, C. L. Korzeniewski, S. Wang and Z. Fan, *ACS Appl. Mater. Interfaces*, 2012, **4**, 3944-3950.
69. A. Leelavathi, G. Madras and N. Ravishankar, *Phys. Chem. Chem. Phys.*, 2013, **15**, 10795-10802.
70. A. Leelavathi, B. Mukherjee, C. Nethravathi, S. Kundu, M. Dhivya, N. Ravishankar and G. Madras, *RSC Adv.*, 2013, **3**, 20970-20977.
71. E. A. Anumol, P. Kundu, P. A. Deshpande, G. Madras and N. Ravishankar, *ACS nano*, 2011, **5**, 8049-8061.

Graphical Abstract

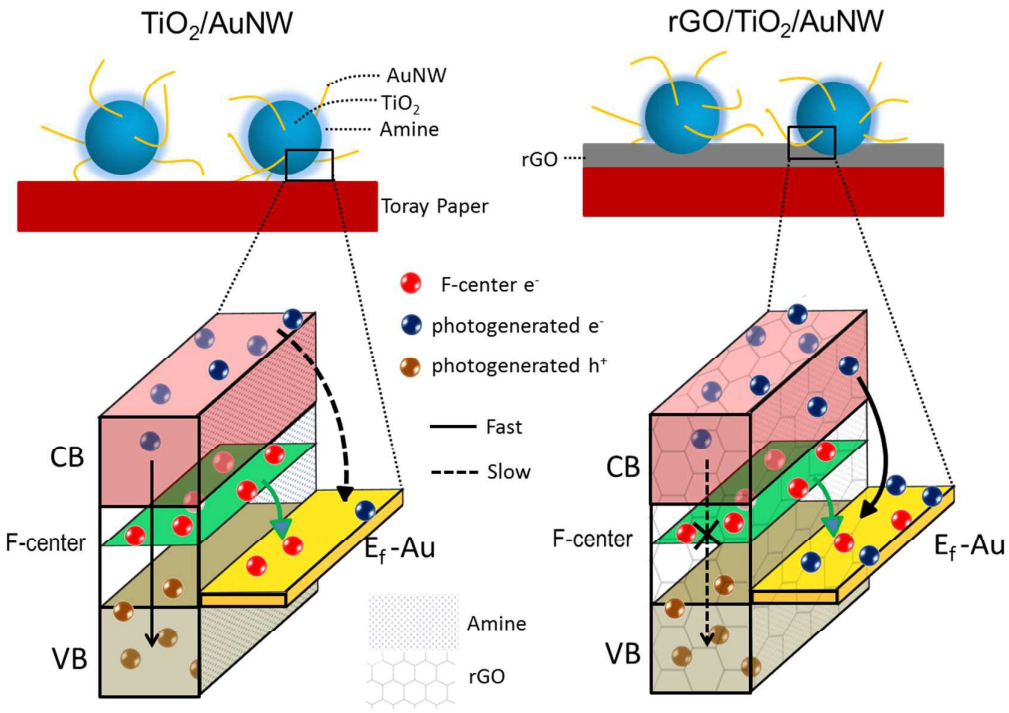

A method to grow ultrathin Au nanowires and metal oxide on reduced graphene oxide (rGO) to produce a hybrid that exhibits good activity for ethanol oxidation.